DOI: 10.1002/cctc.201100160

Tailoring the Activity for Oxygen Evolution Electrocatalysis on Rutile TiO_2(110) by Transition-Metal Substitution

Mónica García-Mota,[a] Aleksandra Vojvodic,[b] Horia Metiu,[c] Isabela C. Man,[d] Hai-Yan Su,[d] Jan Rossmeisl,[d] and Jens K. Nørskov*[a, b, d]

The oxygen evolution reaction (OER) on the rutile M–TiO_2(110) (M = V, Nb, Ta, Cr, Mo, W, Mn, Fe, Ru, Ir, Ni) surfaces was investigated by using density functional theory calculations. The stability of different doped TiO_2 systems was analyzed. The scaling relationship between the binding energies of OER intermediates (HOO* versus HO*) is found to follow essentially the same trend as for undoped oxides. Our theoretical analysis shows a lower overpotential associated with OER on the doped M–TiO_2(110) than on the undoped TiO_2(110). The theoretical activity of Cr-, Mo-, Mn-, and Ir-doped TiO_2 is found to be close to that of RuO_2(110) for some of the configurations in consideration.

Introduction

Electrochemical water splitting is of considerable interest as a key process in hydrogen production from sunlight and other sources of electricity.[1] If the electrical energy is provided by sustainable sources, such as wind, water, or sun, the hydrogen produced is a clean and CO_2-free energy carrier, which can be used in connection with fuel cells to produce energy for a range of applications.[2] Unfortunately, electrochemical water splitting is associated with substantial energy loss mainly because of the high overpotential at the oxygen-evolving anode.[3–5] Therefore, it is important to find the optimal oxygen-evolving electrocatalyst to minimize the energy loss. The most common catalysts used for oxygen evolution reaction (OER) are IrO_2 and RuO_2, which leaves ample room for improvement in terms of price. Co oxides have been suggested as a cheaper alternative, but all these materials have quite a large overpotential for OER.[4] Recently, Marshall et al. developed an $Ir_xRu_yTa_zO_2$ system used as the anode electrocatalyst for proton-exchange membrane (PEM) electrolyzer systems.[6] The lowest overpotential achieved was 0.4 V at 1 A cm^{-2}.

Titanium dioxide (TiO_2) is used as an additive to stabilize active RuO_2 and/or IrO_2 anodes,[3] and it has also been studied as a catalyst for the photoelectrolysis of water.[7] Theoretical work suggests that rutile TiO_2(110) has a very high overpotential for the OER. The reason why TiO_2 can be used as a photocatalyst is because it has a high band gap and, therefore, a high free energy of the holes, which can be used for water splitting.[8]

Numerous studies show that doping improves the catalytic activity of the host oxide. For example, doping RuO_2 with Zn increases the selectivity toward OER in the presence of chlorides by selective suppression of the chlorine evolution reaction.[9] A well-chosen doped rutile TiO_2(110) catalyzes the CO oxidation,[10] and TiO_2 doped with Li, Na, K, and Cs catalyzes acetone oligomerization.[11] Impurity doping is also one of the most promising techniques for improving the activity of TiO_2-based photoelectrolysis cells.[12] However, the doping effect on the oxygen evolution electrocatalysis has not been explored previously. This is the aim of the present theoretical study.

Computational Methods

Calculation details

The effect on the OER overpotential by doping the rutile TiO_2(110) surface was investigated by using first-principles density functional theory (DFT) calculations combined with the computational standard hydrogen electrode (SHE) model.[13] The grid-based projector-augmented wave method (GPAW) code was employed,[14] with the revised Perdew–Burke–Ernzerhof (RPBE) exchange-correlation functional.[15] Inner cores were replaced by using projector-augmented wave method (PAW) pseudopotentials,[16] and a uniform real-spaced grid with a spacing of 0.2 Å was used for the representation of the electronic wave functions. The slabs contained four Ti layers in a (1×2) supercell and were separated by more than 16 Å of vacuum. The *k*-point sampling consisted of 4×4×1 Monkhorst–Pack points.[17] The adsorbates (O*, HO*, and HOO*, in which the asterisk corresponds to an active site on the oxide) together with the two top layers were allowed to relax, whereas the lowest layers were kept frozen at their bulk positions. Spin-polarized cal-

[a] Dr. M. García-Mota, Prof. J. K. Nørskov
Department of Chemical Engineering, Stanford University
Stauffer III, 381 North-South Mall, Stanford, CA 94305 (USA)
Fax: (+1) 650-926-4100
E-mail: norskov@stanford.edu

[b] Dr. A. Vojvodic, Prof. J. K. Nørskov
SUNCAT Center for Interface Science and Catalysis
SLAC National Accelerator Laboratory
2575 Sand Hill Road, Menlo Park, CA 94025 (USA)

[c] Prof. H. Metiu
Department of Chemistry and Biochemistry
University of California, Santa Barbara, CA 93106 (USA)

[d] Dr. I. C. Man, H.-Y. Su, Prof. J. Rossmeisl, Prof. J. K. Nørskov
Department of Physics, Center for Atomic-scale Materials Design
Technical University of Denmark, DK-2800 Kgs. Lyngby (Denmark)

Supporting Information for this article is available on the WWW under http://dx.doi.org/10.1002/cctc.201100160.

culations were performed. The magnetic moment of the isolated dopant was used as the initial guess of the magnetic moment of the dopant in the doped TiO_2(110). The magnetic moment was relaxed during the self-consistency cycles. A dipole correction was applied. All calculations were performed using the ASE simulation package.[18]

Structures of the doped rutile TiO_2(110) surfaces

The doped rutile TiO_2(110) surfaces were simulated by using a substitutional model with 6.25% transition-metal impurities relative to the host Ti atoms in the slab, that is, M–$Ti_{15}O_{32}$. We considered the transition metals M = V, Nb, Ta, Cr, Mo, W, Mn, Fe, Ru, Ir, and Ni as dopants at four different substitutional sites (Figure 1). In the top-most surface layer, either a five-coordinated (5c-M) or a six-coordinated (6c-M) Ti atom was replaced by the dopant M. The substitution of a six-coordinated Ti atom in two different positions in the second surface layer was also considered. Most of the transition-metal oxides were stable under the rutile form.[19] The doped TiO_2 surfaces considered here did not show any substantial surface reconstruction.

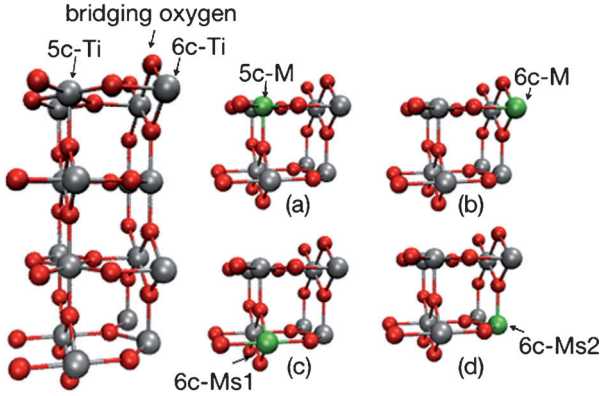

Figure 1. Side view of the $Ti_{16}O_{32}$(110) surface used in the DFT calculations (structure on the left hand side). The bridging oxygen atoms, the five-coordinated atoms (5c-Ti), and the six-coordinated titanium atoms (6c-Ti) are indicated in the figure. On the right hand side, the side views of the two top-most layers of the modeled-doped M–$Ti_{15}O_{32}$ surface are shown. The dopant M is substituting an a) five-coordinated Ti atom (5c-M) and b) six-coordinated Ti atom (6c-M) in the surface layer. Two possible substitutions of a six-coordinated Ti atom are considered in the subsurface layer, denoted as 6c-Ms1 (c) and 6c-Ms2 (d).

The active site on the doped surfaces was the five-fold coordinately unsaturatedsite (CUS). If the dopant is five-coordinated (5c-M), (Figure 1a), the adsorption of the species on the dopant was found to be favored as compared to the adsorption on-top of the fivefold coordinated Ti (see Table S3 in the Supporting Information). In this case, the dopant was considered to be the active site.

Results and Discussion

Free-energy diagram

The water splitting reaction can be written as Equation (1):

$$H_2O(l) \rightarrow 1/2\,O_2(g)+H_2(g) \quad (1)$$

Hydrogen is produced at the cathode and oxygen evolves at the anode. We consider the following four-electron reactions [Eqs. (1a) to (1d)] for the OER in an acidic environment:

$$H_2O(l)+* \rightarrow HO*+H^+ +e^- \quad (1a)$$

$$\Delta G_1^{OER} = \Delta G_{HO*} - eU + k_B T \ln a_{H+}$$

$$HO* \rightarrow O*+H^+ +e^- \quad (1b)$$

$$\Delta G_2^{OER} = \Delta G_{O*} - \Delta G_{HO*} - eU + k_B T \ln a_{H+}$$

$$O*+H_2O(l) \rightarrow HOO*+H^+ +e^- \quad (1c)$$

$$\Delta G_3^{OER} = \Delta G_{HOO*} - \Delta G_{O*} - eU + k_B T \ln a_{H+}$$

$$HOO* \rightarrow *+O_2(g)+H^+ +e^- \quad (1d)$$

$$\Delta G_4^{OER} = 4.92 - \Delta G_{HOO*} - eU + k_B T \ln a_{H+}$$

A more detailed derivation of these expressions can be found in Ref. [8]. The free-energy differences ΔG_{1-4}^{OER} are calculated by using the computational standard hydrogen electrode (SHE).[13] The sum of the free energy of the reaction steps equals the formation energy of O_2 (4.92 eV). At standard conditions (pH 0, $P = 0.1$ MPa, $T = 298$ K) and $U = 0$ V vs. SHE, a proton and an electron are replaced by half a hydrogen molecule. The free energy of the intermediates along the reaction path, ΔG_{HO*}, ΔG_{O*}, and ΔG_{HOO*}, are calculated relative to H_2O and H_2 in the gas phase at $U = 0$ V, standard conditions, and a fixed "standard" coverage of half of the adsorbate species. The free-energy diagrams do not include the barriers between the intermediates. Our analysis can be viewed as a first step toward a complete picture of the reaction path. Calculations for the oxygen reduction reaction (ORR, the reverse reaction of the OER) also indicate that additional barriers are small and independent of potential.[20]

A very important parameter, which can be deduced from the free-energy diagram, is the size of the potential-determining step. This concept was developed and reviewed in previous papers for OER and ORR.[8,13,21–23] The potential-determining step is the highest free-energy step (G^{OER}) in the process and, therefore, the last step to become downhill in free energy as the potential increases. The theoretical overpotential (η^{OER}) at standard conditions is defined as Equation (2):

$$\eta^{OER} = (G^{OER}/e) - 1.23\ V \quad (2)$$

Linear relations and OER activity on undoped oxides

In a previous study, trends in the electrocatalytic activity of the OER were investigated on the basis of a large database of HO* and HOO* adsorption energies on oxide surfaces.[21,24] There is an almost constant difference between the binding energies of the two intermediates: $\Delta G_{HOO*} - \Delta G_{HO*} \approx 3.2$ eV (Figure 2a). An ideal catalyst with zero theoretical overpotential for each step would have $\Delta G_{HOO*} - \Delta G_{HO*} = 2 \times 1.23$ eV $= 2.46$ eV. Therefore, either step 2 or 3 [reactions given by Equations (1b) and (1c),

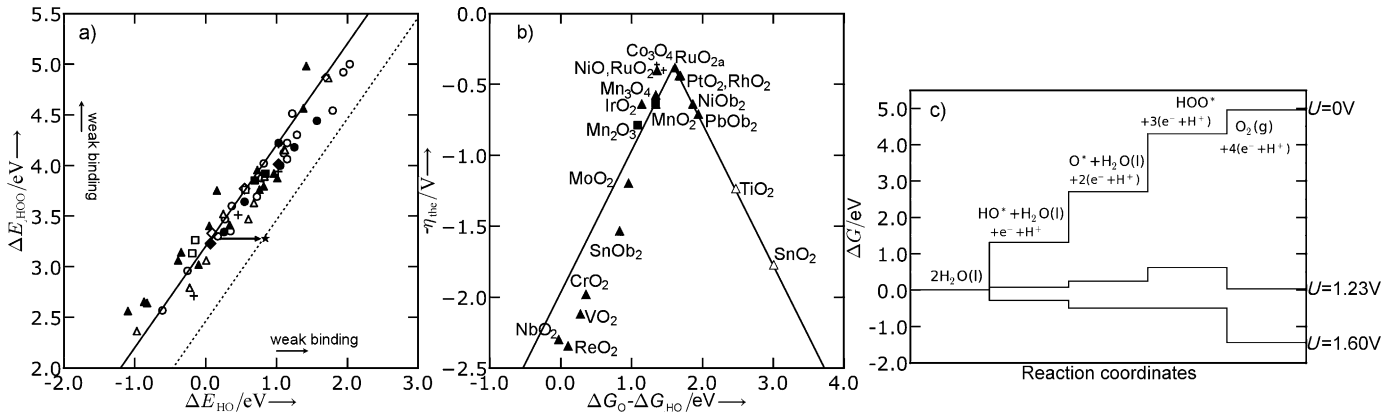

Figure 2. a) Adsorption energies of HOO* as a function of adsorption energies of HO* on rutile (△), perovskites (○), anatase (◇), Mn_xO_y (□), Co_3O_4 (+), and NiO (+) oxides. Open and solid symbols represent the adsorption energies on clean surfaces and on high-coverage surfaces, respectively. The star represents the binding energies required for an ideal electrocatalyst. The dotted line represents the relationship between ΔE_{HOO} and ΔE_{HO*} for an ideal catalyst, which is given by $\Delta E_{HOO*} = \Delta E_{HO*} + 2.44$ eV. The data are taken from Ref. [24]. b) Activity trends toward oxygen evolution for rutile oxides (△), Co_3O_4 (+), and Mn_xO_y (■). Open and solid symbols represent the same surface coverage as Figure 2a. The negative value of the theoretical overpotential is plotted as a function of the standard free energy of $\Delta G_{O*} - \Delta G_{HO*}$. The data are taken from Ref. [24]. c) Standard free-energy diagram for the OER on O*-covered RuO_2 at three different potentials: $U = 0$, 1.23, and 1.60 V. The data are taken from Ref. [22b].

respectively] is likely the potential determining step. That implies that the variation in η^{OER} from one oxide surface to another is determined by the O* adsorption energy, since that determines ΔG_2^{OER} and ΔG_3^{OER} [Eq. (3)]:

$$\begin{aligned} G^{OER} &= \mathrm{Max}[\Delta G_2, \Delta G_3] \\ &= \mathrm{Max}[(\Delta G_{O*} - \Delta G_{HO*}), (\Delta G_{HOO*} - \Delta G_{O*})] \\ &\approx \mathrm{Max}[(\Delta G_{O*} - \Delta G_{HO*}), 3.2\ \mathrm{eV} - (\Delta G_{O*} - \Delta G_{HO*})] \end{aligned} \quad (3)$$

The energy $\Delta G_{O*} - \Delta G_{HO*}$ is, therefore, a descriptor for the OER activity, and the theoretical overpotential at standard conditions is given by Equation (4):

$$\begin{aligned} \eta^{OER} = \{&\mathrm{Max}[(\Delta G_{O*} - \Delta G_{HO*})/e, 3.2\ \mathrm{eV} \\ &- (\Delta G_{O*} - \Delta G_{HO*})/e\} - 1.23\ \mathrm{V} \end{aligned} \quad (4)$$

By plotting η^{OER} as a function of $\Delta G_{O*} - \Delta G_{HO*}$, a volcano relationship is established for oxides (Figure 2b). A lower limit for the theoretical OER overpotential of 0.4 ± 0.2 eV is found for the classes of materials considered (the value ± 0.2 eV stems from the standard deviation of the population from $\Delta G_{HOO*} - \Delta G_{HO*} \approx 3.2$ eV). RuO_2 has an OER overpotential of ≈ 0.4 V, with the formation of the intermediate HOO* being the potential-determining step (Figure 2c). Experimental overpotentials depend on the current density, but it was shown in Ref. [24] that they are proportional to the theoretical overpotential. This strongly supports the notion that trends in the electrochemical activity for OER are determined to a first approximation by thermodynamics. As regards the accuracy of generalized gradient approximation GGA) DFT calculations for oxide chemistry, we are aware that many recent articles have suggested that GGA-DFT does not provide the correct electronic structure for the titanium oxides.[25] The current opinion is that a Hubbard U correction improves the description of the band gap of TiO_2.[26] In spite of the uncertainty surrounding the GGA method, we suggest that, until better methods are applicable, this provides the best method to study the trends in the electrocatalytic activity of OER for doped oxides.

Linear relations and OER activity on doped TiO_2(110)

Using the approach described above, the theoretical overpotentials of the M–$Ti_{15}O_{32}$(110) surfaces (M = V, Nb, Ta, Cr, Mo, W, Mn, Fe, Ru, Ir, Ni) are calculated. The binding energies of O* (ΔE_O), HO* (ΔE_{HO}), and HOO* (ΔE_{HOO}) on the surfaces are calculated relative to H_2O and H_2 in the gas phase, because these are well described within DFT (see Table S3 in the Supporting Information). We have considered that only half of the coordinately unsaturated sites are occupied by O*, HO*, or HOO*. We are aware that the binding energies of the species may depend fairly strongly on the concentration; this issue is not addressed here because we are mostly interested in trends. The analysis of the relative stability of different surface coverages relevant to electrolysis will be discussed in future work.

We find that the introduction of dopants leads to a stronger interaction of the adsorbate species with the surface as compared to that on pure TiO_2 for most of the systems under consideration (Figure 3a). The strength is determined by the type of the transitional metal and also by its position in the lattice. The scaling relationship between the binding energies of the OER-intermediates HOO* and HO* follows essentially the same trend as for undoped oxides (Figure 3a). The mean absolute error of the scaling relation including both doped and undoped oxides is 0.17 eV, which is the same as for undoped oxides.

Our theoretical analysis indicates a lower theoretical overpotential associated with OER on the doped M–$Ti_{15}O_{32}$(110) compared to on the undoped TiO_2 (Figure 3b). Either the formation of O* or the formation of the intermediate HOO* is the potential-determining step for OER for most of the systems under

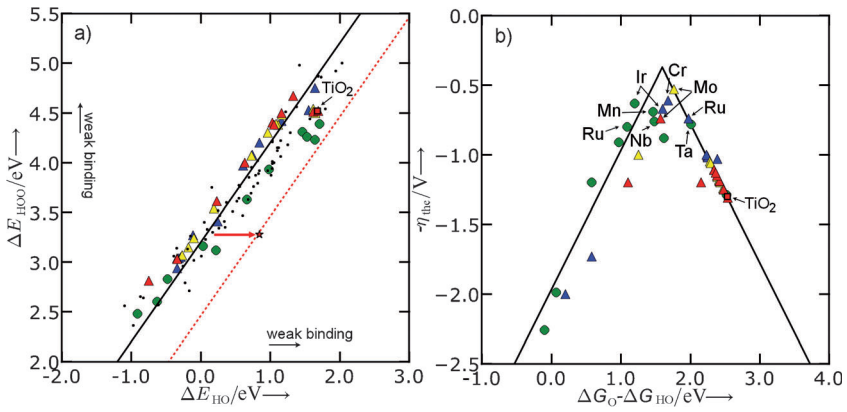

Figure 3. a) Adsorption energies of HOO* as a function of the adsorption energy of HO* on the surfaces of M–$Ti_{15}O_{32}$ (M = V, Nb, Ta, Cr, Mo, W, Mn, Fe, Ru, Ir, Ni, colored points). The small black circles correspond to ΔE_{HOO} as a function of ΔE_{HO} on pure oxides (data taken from Ref. [24]). The red star indicates where the binding energies need to be for an ideal electrocatalyst. b) Calculated theoretical overpotentials plotted as a function of $\Delta G_{O^*}-\Delta G_{HO^*}$ for M–$Ti_{15}O_{32}$. The volcano curve is established by using the scaling relation between $\Delta G_{HOO^*}-\Delta G_{O^*}$ and $\Delta G_{O^*}-\Delta G_{HO^*}$ as described in Ref. [24]. Green circles stand for configurations in which the dopant is five-fold coordinated. Triangles stand for configurations in which the dopant is six-fold-coordinated: 6c-M (blue), 6c-Ms1 (red), and 6c-Ms2 (yellow).

consideration. The only exception is the Mn–$Ti_{15}O_{32}$ alloy with the dopant in the five-coordinated site for which the formation of HO* is the potential-determining step. The correlation found between ΔE_{HOO^*} and ΔE_{HO^*} allows us to use $\Delta G_{O^*}-\Delta G_{HO^*}$ as an activity descriptor of M–$Ti_{15}O_{32}$(110) surfaces as in the case of undoped oxides (Figure 3b). The catalytic activity of some configurations of TiO_2 doped with Cr, Mo, Mn, or Ir is close to that of RuO_2 (Table 1). We found that these are stable configurations with the exception of Ir–TiO_2.

To assess the stability of the doped oxides, the formation energies ΔE_{form} have been calculated according to Equation (5):

$$\Delta E_{form} = E_{M-Ti_{15}O_{32}} - [E_{Ti_{16}O_{32}} + E_{M(bulk)} - E_{TiO_2(bulk)} + \mu_{O_2(g)}] \quad (5)$$

$E_{M-Ti_{15}O_{32}}$ is the energy of the slab with one substituted M atom and $E_{Ti_{16}O_{32}}$ is the energy of the undoped slab. $E_{TiO_2(bulk)}$ and $E_{M(bulk)}$ are the bulk energies of TiO_2 and of the dopant, respectively. $\mu_{O_2(g)}$ is the chemical potential of the O_2 molecule in the gas phase at standard conditions ($T = 298$ K and $P = 0.1$ MPa). Substitutional doping is energetically more favorable the smaller the ΔE_{form} value is. The trend in the formation energy of doped TiO_2 can be understood by considering the electronegativity of the metal that is introduced into the TiO_2 lattice.[10b,27] In most cases, a strong M–O bond is associated with low-electronegativity dopants . Experimentally, the location and the quantity of the dopants in TiO_2 are difficult to predict.[28] A theoretical analysis of segregation and migration effects of the host atom toward the most stable positions caused by different applied potentials and pH is out of the scope of this study.

Our theoretical analysis suggests that doped TiO_2 catalysts would be interesting candidates as low-cost (photo-)electrocatalysts. Doped TiO_2 with Cr, Mo, Fe, Ni, V, Mn, and Cu have been experimentally synthesized and tested for photoelectrochemical water splitting.[12] The observed enhanced photoelectrochemical activity was suggested to be attributable to a better photoresponse of TiO_2 in the visible spectrum because of the additional energy levels that emerge in the band gap of TiO_2. Our calculations suggest that the enhanced photoelectrochemical activity could actually (also) be an effect of increased catalytic activity. We suggest that doped TiO_2, for instance as thin layers (so that electrical conductivity is not an issue), may be a cheap alternative to other transition-metal oxides used as electrocatalysts.

Conclusions

In the present paper, we have performed a study of the effect of doped rutile M–$Ti_{15}O_{32}$(110) (M = V, Nb, Ta, Cr, Mo, W, Mn, Fe, Ru, Ir, Ni) on the (OER) activity. The correlation between the HOO* and HO* energies essentially follow the same trend as the one found for undoped oxides. We have found that transition-metal-doped TiO_2 has a lower overpotential than the undoped TiO_2. The OER activity is considerably enhanced for Cr-, Mo-, Mn- and Ir-doped TiO_2(110). The systems considered herein provide no better catalysts than known catalysts, but given that TiO_2 is extremely cheap they may serve as candidates for inexpensive alternatives, if it is possible to synthesize and couple them to an electrode or a suitable photon absorber.

Table 1. Binding energies of O*, HO*, and HOO* (ΔE_{O^*}, ΔE_{HO^*}, and ΔE_{HOO^*}), potential-determining step (pds) (either O*, HO*, or HOO* formation), and theoretical overpotential (η^{OER}) associated with OER on doped M–$Ti_{15}O_{32}$.[a]

Dopant	Coordination	ΔE_{form} [eV]	ΔE_{O^*} [eV]	ΔE_{HO^*} [eV]	ΔE_{HOO^*} [eV]	pds	η^{OER} [V]
Nb	5c-M	−5.15	1.26	−0.48	2.83	HOO*	0.76
Ta	5c-M	−5.80	1.37	−0.91	2.48	O*	0.78
Cr	6c-M	−3.82	2.78	0.84	4.20	HOO*	0.61
Mo	6c-Ms1	−3.15	2.06	0.23	3.61	HOO*	0.74
	6c-Ms2	−3.37	2.22	0.19	3.54	O*	0.53
Mn	5c-M	−3.53	3.26	1.53	4.26	HO*	0.69
Ru	5c-M	−0.27	2.02	0.66	3.63	HOO*	0.80
	6c-M	−0.57	2.85	0.61	3.97	O*	0.74
Ir	5c-M	+0.56	1.68	0.22	3.12	HOO*	0.63
	6c-M	+0.04	2.60	0.74	4.08	HOO*	0.67

[a] Only configurations that have a η^{OER} lower than 0.8 V are compiled in this table. The position of the dopant in the TiO_2 lattice is indicated (see labels in Figure 1). Formation energies (ΔE_{form}) were calculated by using Eq. (5).

Acknowledgements

M.G.M. and J.K.N. acknowledge support from the Center of Nanostructuring for Efficient Energy Conversion (CNEEC) at Stanford University, an Energy Frontier Research Center funded by the U.S. Department of Energy, Office of Basic Energy Sciences under award number DE-SC0001060 for OER calculations. A.V. and J.K.N. acknowledge support from the Center for Interface Science and Catalysis (SUNCAT) through the U.S. Department of Energy, Office of Basic Energy Sciences for general scaling relations for oxides. J.R., I.C.M., and H.-Y.S. acknowledge the Catalysis for Sustainable Energy (CASE) initiative, the Danish Strategic Research Council's HyCycle program, and the Danish Council for Technology and Innovation's FTP program for OER calculations.

Keywords: density functional calculations · heterogeneous catalysis · scaling · surface chemistry · water splitting

[1] J. O. Bockris, *Int. J. Hydrogen Energy* **2008**, *33*, 2129 – 2131.
[2] M. S. Dresselhaus, I. L. Thomas, *Nature* **2001**, *414*, 332 – 337.
[3] a) S. Trasatti, *Electrochim. Acta* **1984**, *29*, 1503 – 1512; b) S. Trasatti, *Electrochim. Acta* **1991**, *36*, 225 – 241.
[4] M. Hamdani, R. N. Singh, P. Chartier, *Int. J. Electrochem. Sci.* **2010**, *5*, 556 – 577.
[5] B. A. Pinaud, Z. Chen, D. N. Abram, T. F. Jaramillo, *J. Phys. Chem. C* **2011**, *115*, 11 830 – 11 838
[6] A. T. Marshall, S. Sunde, M. Tsypkin, R. Tunold, *Int. J. Hydrogen Energy* **2007**, *32*, 2320 – 2324.
[7] a) M. Grätzel, *Nature* **2001**, *414*, 338 – 344; b) A. Fujishima, K. Honda, *Nature* **1972**, *238*, 37 – 38; c) A. L. Linsebigler, G. Lu, J. T. Yates, *Chem. Rev.* **1995**, *95*, 735 – 758.
[8] Á. Valdés, Z. W. Qu, G. J. Kroes, J. Rossmeisl, J. K. Nørskov, *J. Phys. Chem. C* **2008**, *112*, 9872 – 9879.
[9] a) H. A. Hansen, I. C. Man, F. Studt, F. Abild-Pedersen, T. Bligaard, J. Rossmeisl, *Phys. Chem. Chem. Phys.* **2010**, *12*, 283 – 290; b) V. Petrykin, K. Macounova, O. A. Shlyakhtin, P. Krtil, *Angew. Chem.* **2010**, *122*, 4923 – 4925; *Angew. Chem. Int. Ed.* **2010**, *49*, 4813 – 4815.
[10] a) S. Chrétien, H. Metiu, *Catal. Lett.* **2006**, *107*, 143 – 147; b) H. Y. Kim, H. M. Lee, R. G. S. Pala, V. Shapovalov, H. Metiu, *J. Phys. Chem. C* **2008**, *112*, 12398 – 12408.
[11] M. Zamora, T. López, R. Gómez, M. Asomoza, R. Melendrez, *Catal. Today* **2005**, *107*, 289 – 293.
[12] a) M. Radecka, M. Wierzbicka, S. Komornicki, M. Rekas, *Physica B* **2004**, *348*, 160 – 168; b) L. G. Devi, B. N. Murthy, *Catal. Lett.* **2008**, *125*, 320 – 330; c) R. Dholam, N. Patel, M. Adami, A. Miotello, *Int. J. Hydrogen Energy* **2009**, *34*, 5337 – 5346; d) W.-J. Yin, T. Houwen, S.-H. Wei, M. Mowafak, J. T. Al-Jassim, Y. Yanfa, *Phys. Rev. B* **2010**, *82*, 045106.
[13] J. K. Nørskov, J. Rossmeisl, A. Logadottir, L. Lindqvist, J. R. Kitchin, T. Bligaard, H. Jonsson, *J. Phys. Chem. B* **2004**, *108*, 17 886 – 17 892.
[14] J. Enkovaara, C. Rostgaard, J. J. Mortensen, J. Chen, M. Dulak, L. Ferrighi, J. Gavnholt, C. Glinsvad, V. Haikola, H. A. Hansen, H. H. Kristoffersen, M. Kuisma, A. H. Larsen, L. Lehtovaara, M. Ljungberg, O. Lopez-Acevedo, OP. G. Moses, J. Ojanen, Y. Olsen, TV. Petzold, N. A. Romero, J. Stausholm-Møller, M. Strange, G. A. Tritsaris, M. Vanin, M. Walter, B. Hammer, H. Hakkinen, G. Madsen, R. M. Nieminen, J. K. Nørskov, M. Puska, T. T. Rantala, J. Schiotz, K. Thygesen, K. W. Jacobsen, *J. Phys. Condens. Matter* **2010**, *22*, 253202.
[15] B. Hammer, L. B. Hansen, J. K. Nørskov, *Phys. Rev. B* **1999**, *59*, 7413.
[16] G. Kresse, D. Joubert, *Phys. Rev. B* **1999**, *59*, 1758 – 1775.
[17] H. J. Monkhorst, J. D. Pack, *Phys. Rev. B* **1976**, *13*, 5188 – 5192.
[18] S. R. Bahn, K. W. Jacobsen, *Comput. Sci. Eng.* **2002**, *4*, 56 – 66.
[19] J. I. Martínez, H. A. Hansen, J. Rossmeisl, J. K. Nørskov, *Phys. Rev. B* **2009**, *79*, 045 120 – 045 125.
[20] V. Tripkovic', E. Sku'lasona, S. Siahrostamia, J. K. Nørskov, J. Rossmeisl, *Electrochim. Acta* **2010**, *55*, 7975 – 7998.
[21] M. T. M. Koper, *J. Electroanal. Chem.* **2010**, in press, DOI:10.1016/j.jelechem.2010.10.004.
[22] a) J. Rossmeisl, A. Logadottir, J. K. Nørskov, *Chem. Phys.* **2005**, *319*, 178 – 184; b) J. Rossmeisl, Z. W. Qu, H. Zhu, G. J. Kroes, J. K. Nørskov, *J. Electroanal. Chem.* **2007**, *607*, 83 – 89.
[23] H. Dau, C. Limberg, T. Reier, M. Risch, S. Roggan, P. Strasser, *ChemCatChem* **2010**, *2*, 724 – 761.
[24] I. C. Man, H. Y. Su, F. Calle-Vallejo, H. A. Hansen, J. I. Martínez, N. G. Inoglu, J. Kitchin, T. F. Jaramillo, J. K. Nørskov, J. Rossmeisl, *ChemCatChem* **2011**, *3*, 1159 – 165.
[25] a) G. Pacchioni, *J. Chem. Phys.* **2008**, *128*, 182505 – 182510; b) M. V. Ganduglia-Pirovano, A. Hofmann, J. Sauer, *Surf. Sci. Rep.* **2007**, *62*, 219 – 270.
[26] a) N. J. Mosey, E. A. Carter, *Phys. Rev. B* **2007**, *76*, 155 123; b) Y.-L. Lee, J. Kleis, J. Rossmeisl, D. Morgan, *Phys. Rev. B* **2009**, *80*, 224 101; c) Z. Hu, H. Metiu, *J. Phys. Chem. C* **2011**, *115*, 5841 – 5845; d) S. Chrétien, H. Metiu, *J. Phys. Chem. C* **2011**, *115*, 4696 – 4705.
[27] a) K. Yang, Y. Dai, B. Huang, M. H. Whangbo, *Chem. Mater.* **2008**, *20*, 6528 – 6534; b) R. Long, Y. Dai, G. Meng, B. Huang, *Phys. Chem. Chem. Phys.* **2009**, *11*, 8165 – 8172.
[28] a) A. Kubacka, G. Colon, M. Fernandez-Garcia, *Catal. Today* **2009**, *143*, 286 – 292; b) M. Hrovat, J. Holc, Z. Samardžija, G. Dražič, *J. Mater. Res.* **1996**, *11*, 727 – 732; c) K. T. Jacob, R. Subramanian, *J. Phase Equilib. Diffus.* **2008**, *29*, 136 – 140.

Received: May 13, 2011
Published online on August 25, 2011

